Membrane Topology of the Human Breast Cancer Resistance Protein (BCRP/ABCG2) Determined by Epitope Insertion and Immunofluorescence[†]

Honggang Wang,[‡,§] Eun-Woo Lee,[‡,§,||] Xiaokun Cai,[§] Zhanglin Ni,[§] Lin Zhou,[§] and Qingcheng Mao*[,§]

Department of Pharmaceutics, School of Pharmacy, University of Washington, Seattle, Washington 98195, and Department of Life Science and Biotechnology, College of Natural Science, Dongeui University, Busan 614-714, Korea

Received August 29, 2008; Revised Manuscript Received November 12, 2008

ABSTRACT: The human breast cancer resistance protein (BCRP/ABCG2) mediates efflux of drugs and organic anions across the plasma membrane. Hydropathy analysis suggests that BCRP consists of a nucleotide-binding domain (residues ~1−395) and a membrane-spanning domain (MSD) (residues ~396−655); however, its exact topology structure remains unknown. In this study, we determined the topology structure of BCRP by inserting hemagglutinin (HA) tags in its predicted hydrophilic regions of the MSD. HA-tagged BCRP mutants were expressed in HEK cells and tested for their ability to efflux mitoxantrone and BODIPY-prazosin. Polarity of the inserted tags with respect to the plasma membrane was determined by immunofluorescence. All of the mutants were expressed at levels comparable to wild-type BCRP as revealed by immunoblotting with specific antibodies against BCRP and the HA tag. Insertions at residues 423, 454, 462, 499, 529, 532, and 651 produced functional mutants, whereas insertions at residues 560, 594, and 623 resulted in mutants with significantly reduced activity and insertions at residues 387, 420, 474, and 502 completely abrogated the activity. HA tags inserted at residues 387, 474, 529, 532, 560, and 651 were localized intracellularly, whereas those inserted at residues 420, 423, 454, 499, 502, 594, and 623 revealed an extracellular location. Residue 462 was localized in a transmembrane (TM) segment. These results provide the first direct experimental evidence in support of a 6-TM model for BCRP with the amino and carboxyl termini of the MSD located intracellularly. These data may have important implications for understanding the transport mechanism of BCRP.

The breast cancer resistance protein (BCRP)[1] is an approximately 75 kDa polytopic integral plasma membrane transporter belonging to subfamily G of the large human ATP-binding cassette (ABC) transporter superfamily. BCRP is the second member of subfamily G and hence designated as ABCG2. BCRP is considered to be one of the most important ABC efflux transporters that confers multidrug resistance in cancer cells owing to its ability to efflux chemotherapeutic agents out of the cell (*1*−*5*). Functional studies in the past decade have suggested that BCRP can transport a broad spectrum of substrates, ranging from hydrophobic chemotherapeutics to hydrophilic organic anions (*6*−*9*). With respect to tissue localization, BCRP has been shown to be highly expressed in the apical membrane of the placental syncytiotrophoblasts, the small intestinal epithelium, the liver canaliculi, and the brain blood vessel capillaries (*2, 10*). Therefore, BCRP is also increasingly recognized for its role in regulating drug disposition and xenobiotic exposure owing to its broad substrate specificity and the pattern of tissue expression (*6, 7*). The importance of BCRP for the absorption (intestinal), distribution (e.g., across placental and blood-brain barriers), and elimination (hepatic) of substrate drugs has been demonstrated in numerous studies (*11*−*18*). In addition, BCRP in the apical membrane of mammary alveolar epithelia has been shown to be responsible for the efflux of xenobiotics/drugs and vitamins into breast milk (*19, 20*).

BCRP is a medically important ABC efflux transporter. At present, our knowledge regarding the structure−function relationship and transport mechanism of BCRP is limited. It has been proposed that BCRP may function as a homodimer or homooligomer (*21*−*23*). Mutation analysis in the past several years also identified various amino acid residues that seem to be important for the overall transport activity, substrate selectivity, processing, or trafficking of BCRP (*24*−*32*). In particular, amino acid substitution at position 482 of BCRP has been shown to be absolutely critical for substrate specificity and transport activity (*27, 29, 30, 33*). However, since a high-resolution structure of BCRP has not been obtained so far (*22, 34*), it remains elusive to explain the currently available biochemical data. As one of the efforts toward the understanding of the structural basis of BCRP action, the goal of this study was to elucidate the topological

[†] This work was supported by a grant from the National Institutes of Health, GM073715 (to Q.M.).

* Address correspondence to this author. Tel: 206-685-0355. Fax: 206-543-3204. E-mail: qmao@u.washington.edu.

[‡] The first two authors equally contributed to this work.

[§] University of Washington.

[||] Dongeui University.

[1] Abbreviations: BCRP, breast cancer resistance protein; ABC, ATP-binding cassette; ABCG2, ATP-binding cassette G2; NBD, nucleotide-binding domain; MSD, membrane-spanning domain; TM, transmembrane; HEK, human embryonic kidney; FTC, fumitremorgin C; MX, mitoxantrone; HA, hemagglutinin; ANOVA, analysis of variance; mAb, monoclonal antibody; DMSO, dimethyl sulfoxide; MEM, Eagle's minimum essential medium; FBS, fetal bovine serum; PBS, phosphate-buffered saline; WT, wild type; PCR, polymerase chain reaction; LB, Luria−Bertani; SDS, sodium dodecyl sulfate.

10.1021/bi801644v CCC: $40.75
Published on Web 12/08/2008

structure of BCRP. At present, the membrane topology of BCRP remains largely unknown. Topology models have been proposed for BCRP using bioinformatics tools (*1, 4, 5, 34, 35*). For example, hydropathy analysis of its deduced amino acid sequence predicted that BCRP contains a nucleotide-binding domain (NBD) (residues ~1−395) followed by a MSD (residues ~396−655) with 6 transmembrane (TM) segments (*1, 4, 5*). The recent homology modeling study based on the published crystal structure of the multidrug transporter Sav1866 from *Staphylococcus aureus* also predicted a similar topology structure of BCRP as the hydropathy analysis (*34*). However, these computer-generated topology models have not been confirmed by experimental data. Further experimental studies are thus essential to determine the exact number and arrangement of TM segments, the location of hydrophilic loops connecting the TM segments, and the orientation of the amino and carboxyl termini of the MSD of BCRP.

In the present study, we have performed epitope insertion and immunofluorescence to determine the membrane topology of BCRP. Hemagglutinin (HA) epitope tags were inserted in the predicted hydrophilic regions of the MSD of BCRP by insertion mutagenesis. The HA-tagged BCRP mutants were expressed in HEK cells by transient transfection. Expression and efflux activities of these mutants were analyzed by immunoblotting and flow cytometric efflux assay, respectively. Polarity of the inserted HA tags with respect to the plasma membrane (intracellular or extracellular) was then determined by immunofluorescence in intact and permeabilized cells using an HA tag-specific monoclonal antibody. Such an epitope insertion and indirect immunofluorescence approach has been widely used to define the membrane topology of a variety of integral membrane proteins, including the medically important ABC transporters (*36*−*39*).

EXPERIMENTAL PROCEDURES

Materials. BODIPY FL-prazosin (BODIPY-prazosin) was purchased from Molecular Probes (Eugene, OR). Mitoxantrone (MX) was obtained from Sigma (St. Louis, MO). Fumitremorgin C (FTC) was obtained from the National Cancer Institute (Bethesda, MD). HEK293 cells were purchased from American Type Culture Collection (Manassas, VA). Eagle's minimum essential medium (MEM) was from Hyclone (Waltham, MA). Fetal bovine serum (FBS), phosphate-buffered saline (PBS), and trypsin-EDTA solution were from Invitrogen (Carlsbad, CA). FuGENE HD transfection reagent was from Roche Applied Science (Indianapolis, IN). All restriction enzymes were from New England Biolabs (Beverly, MA). Oligonucleotides used for mutagenesis were ordered from Integrated DNA Technologies (Coralville, IA). The monoclonal mouse anti-HA antibody 12CA5 and the anti-mouse IgG_{2b} (γ2b) peroxidase antibody were from Roche Applied Science. The monoclonal mouse anti-BCRP antibody BXP-21 was from Kamiya Biomedical Co. (Seattle, WA). The polyclonal rabbit anti-BCRP antibody was from Proteintech Group, Inc. (Chicago, IL). The monoclonal goat anti-mouse and goat anti-rabbit HRP-conjugated antibodies were purchased from Bio-Rad (Hercules, CA). Alexa-Fluor488 goat anti-mouse IgG (H + L) was obtained from Invitrogen. The pcDNA3.1 plasmid containing full-length wild-type human *BCRP* cDNA was kindly provided by Dr. Susan Bates (National Cancer Institute, Bethesda, MD).

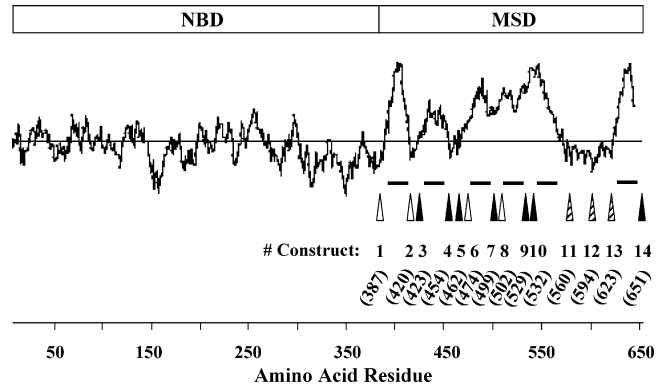

FIGURE 1: Hydropathy analysis of BCRP. Hydropathy analysis of BCRP was performed according to Kyte and Doolittle (*47*). Schematic presentations of the hydropathy profile, putative NBD and MSD, and approximate amino acid positions are shown. Solid bars indicate potential TM segments with approximately 20 amino acids in length. Approximate locations of HA tags inserted in the predicted hydrophilic regions of the MSD are illustrated by arrows. Solid, hatched, and open arrows indicate that HA tag insertions resulted in functional (with 50% or more of wild-type BCRP activity), partially functional (with less than 50% of wild-type BCRP activity), and inactive BCRP mutants, respectively. The corresponding constructs are shown in numbers 1−14, and amino acid residues immediately preceding the HA tags are provided in parentheses.

PCR-Based Epitope Insertion Mutagenesis. HA epitope tags were inserted at 14 discrete locations in BCRP as 9 amino acid peptides (YPYDVPDYA) by inverted PCR mutagenesis as previously described (*38, 40*). The locations of HA tags were selected in the predicted hydrophilic regions of the MSD of BCRP based on hydropathy analysis of the amino acid sequence of BCRP (Figure 1). The DNA sequences of primers used for mutagenesis are shown in Table 1. All of the primers were phosphorylated at the 5′ end. Briefly, the full-length wild-type human *BCRP* cDNA cloned into the pcDNA3.1 expression vector was used as the template for mutagenesis. The primers were designed in such a way that the first half of the tag sequence was incorporated at the 5′-end of the upstream primer and the second half of the tag sequence incorporated into the 5′-end of the downstream primer by PCR. The PCR reaction mixture (50 μL) contained dNTPs (160 μM each NTP), 2.5 units of *Pfu* ultra DNA polymerase (Stratagene, La Jolla, CA), 10−20 ng of template DNA, 5 μL of 10 times concentrated *Pfu* reaction buffer, and 25 pmol of each primer. PCR was performed as follows. Following an initial denaturing at 95 °C for 4 min, the reaction was run for 16 cycles (95 °C for 30 s, 49−60 °C for 30 s, and 72 °C for 20 min) with a final extension at 72 °C for 25 min. The annealing temperature (49−60 °C) varied depending on the melting temperature of each primer. The PCR products were purified using Qiagen PCR purification kit, eluted in 30 μL of elution buffer, and ligated using T4 DNA ligase (New England Biolabs) for 2 h at room temperature followed by heat inactivation of the ligase at 65 °C for 15 min. The ligated product was then incubated with the restriction enzyme *Dpn*I overnight at 37 °C to digest template DNA and cleaned up using the Qiagen PCR purification kit. *Dpn*I-digested DNA was used to transform *Escherichia coli* XL-1 Blue competent cells (Stratagene), and the *E. coli* cells were plated on

Table 1: PCR Primers Designed for HA Tag Insertion Mutagenesis of This Study

construct	insertion site[a]	forward primer (5′ to 3′)[d]	reverse primer (5′ to 3′)[e]
1	N387[b]-L388[c]	X ttg ctg ggt aat ccc cag gcc	Y gtt ttt gaa tga acg ctt gga
2	S420[b]-T421[c]	X act gga atc cag aac aga gct	Y aga atc att ttt tag ccc aaa
3	I423[b]-Q424[c]	X cag aac aga gct ggg gtt ctc	Y gat tcc agt aga atc att ttt
4	L454[b]-F455[c]	X ttc ata cat gaa tac atc agc	Y gag ctt ctt ctc tac cac aaa
5	G462[b]-Y463[c]	X tac tac aga gtg tca tct tat	Y tcc gct gat gta ttc atg tat
6	L474[b]-L475[c]	X tta tct gat tta tta ccc atg	Y cag ttt tcc aag gaa ata aga
7	L499[b]-K500[c]	X aag cca aag gca gat gcc ttc	Y caa tcc taa cat gaa gta cac
8	K502[b]-A503[c]	X gca gat gcc ttc ttc gtt atg	Y ctt tgg ctt caa tcc taa cat
9	A529[b]-G530[c]	X ggt cag agt gtg gtt tct gta	Y tgc tgc tat ggc cag tgc cat
10	S532[b]-V533[c]	X gtg gtt tct gta gca aca ctt	Y act ctg acc tgc tgc tat ggc
11	T560[b]-I561[c]	X att gca tct tgg ctg tca tgg	Y ggt tgt gag att gac caa cag
12	G594[b]-L595[c]	X ctc aat gca aca gga aac aat	Y tcc tgg gca gaa gtt ttg tcc
13	P623[b]-W624[c]	X tgg ggc ttg tgg aag aat cac	Y ggg tga gag atc gat gcc ctg
14	L651[b]-K652[c]	X aaa aaa tat tct taa att gga	Y aag aaa taa caa ttt cag gta

[a] Sites of HA tag insertions in the BCRP protein sequence as illustrated in Figure 1. [b] Amino acid residues immediately preceding and following the HA tag (YPYDVPDYA), respectively. [c] Amino acid residues immediately preceding and following the HA tag (YPYDVPDYA), respectively. [d] Forward primer where "X" is the second half of the HA tag sequence, 5′-gtg cct gat tac gcc-3′. [e] Reverse primer where "Y" is the first half of the HA tag sequence, 5′-gtc gta agg gta-3′.

Luria−Bertani (LB) plates containing 100 μg/mL ampicillin. The plates were incubated overnight at 37 °C. Colonies were picked up and grown in LB broth overnight at 37 °C. Plasmids were then isolated from *E. coli* cells using the Qiagen miniprep kit. The pcDNA3.1 constructs containing HA-tagged BCRP mutant cDNAs with correct HA tag insertions were confirmed by DNA sequencing and used for transient transfection into HEK cells.

Cell Culture and Transient Transfection. HEK293 cells were grown and maintained in MEM containing 10% FBS at 37 °C in a humidified incubator with 5% CO_2. For transient transfection, cells were seeded at a density of approximately 5×10^3 cells/cm^2 in MEM on 6 cm dishes (Costar, Corning, NY) for immunoblotting and transport studies or four-chamber tissue culture treated glass slides (BD Falcon, Bedford, MA) for immunofluorescence studies. Approximately 2 μg of plasmid DNA was used to transfect 5×10^4 cells with FuGENE transfection reagent, according to the manufacturer's instruction. Forty-eight hours posttransfection, the cells were used for subsequent studies.

SDS−Polyacrylamide Gel Electrophoresis and Immunoblotting. Forty-eight hours after transfection, cells were trypsinized and washed twice in PBS. Whole cell lysates were then prepared from the cells as described (*41, 42*). Protein concentrations were determined using the Bio-Rad Dc protein assay kit and bovine serum albumin as standard. Protein samples of whole cell lysates (30 μg each lane) were subjected to immunoblotting as previously described (*41, 42*). For detection of BCRP with the BCRP-specific mAb BXP-21, the primary antibody and the secondary goat anti-mouse HRP-conjugate were used at 1:500 and 1:5000 dilution, respectively. For detection of BCRP with a rabbit anti-BCRP polyclonal antibody, the primary antibody and the secondary goat anti-rabbit HRP conjugate were used at 1:2500 and 1:6000 dilution, respectively. For detection of the HA tag, the HA tag-specific mAb 12CA5 and the secondary anti-mouse IgG_{2b} (γ2b) peroxidase were used at 1:500 and 1:4000 dilution, respectively. For detection of β-actin (internal standard), a human β-actin-specific mAb (Sigma) and the secondary goat anti-mouse HRP conjugate were used at 1:50000 and 1:25000 dilution, respectively.

Flow Cytometric Efflux Assay. Flow cytometric efflux assays were performed as previously described (*41, 43*). Two known BCRP substrates, MX and BODIPY-prazosin, and the BCRP-specific inhibitor FTC were used in the efflux assays. Briefly, 48 h after transfection, cells were trypsinized, washed twice in PBS, and suspended in incubation buffer (MEM supplemented with 5% FBS and 5 mM HEPES buffer) at a cell concentration of approximately 10^6 cells per reaction in 1 mL volume. In the accumulation phase, cells were incubated with 10 μM MX or 500 nM BODIPY-prazosin in the presence or absence of 10 μM FTC for 30 min at 37 °C. Cells were then immediately transferred on ice, washed twice with ice-cold PBS, and resuspended in 1 mL of incubation buffer with or without 10 μM FTC but containing no MX or BODIPY-prazosin, and then incubation was continued for 1 h at 37 °C to allow maximum efflux of the fluorescent compounds (efflux phase). Cells were then washed twice with ice-cold PBS, resuspended in 500 μL of ice-cold PBS, and kept on ice in the dark. Intracellular fluorescence was measured within 1 h with a 488 nm argon laser filter and a 650 nm long-pass filter for MX and with a 488 nm argon laser filter and a 530 nm bandpass filter for BODIPY-prazosin in a BD FACScan flow cytometer. Ten thousand (10^4) events were collected for all of the samples. Cell debris was eliminated by gating on forward versus side scatter. The difference in median fluorescence (ΔF) between the FTC/efflux histogram and the efflux histogram was used as a measure of FTC-inhibitable MX or BODIPY-prazosin efflux activity of the cells. This FTC-inhibitable MX or BODIPY-prazosin efflux activity is attributable to BCRP expression and function. MX or BODIPY-prazosin was dissolved in incubation buffer containing 0.2% (v/v) DMSO. No effect of DMSO on efflux activity was observed at this concentration.

Immunofluorescence Microscopy. Transiently transfected HEK cells grown in a four-chamber glass slide were examined 48 h after transfection. For experiments using permeabilized cells, cells were fixed in 4% paraformaldehyde in PBS for 30 min, washed twice with PBS, and then incubated with 0.01% (v/v) Triton X-100 in incubation buffer (5% goat serum and 1% albumin in PBS) at room temperature for 30 min. Cells were then incubated in the same buffer containing the anti-HA mAb 12CA5 (1:100 dilution) for 1 h at room temperature. After the cells were washed three times with incubation buffer, the secondary antibody Alexa-

Fluor488 goat anti-mouse IgG (H + L) was added at 1:1000 dilution and incubated for 30 min at room temperature. For experiments using intact nonpermeabilized cells, cells were fixed in 1% paraformaldehyde in PBS at room temperature for 10 min, washed twice with PBS, and then incubated with the anti-HA antibody (1:100 dilution) in incubation buffer for 1 h at room temperature. After the cells were washed three times with incubation buffer, the secondary antibody Alexa-Fluor488 goat anti-mouse IgG (H + L) was added at 1:1000 dilution and incubated for 30 min at room temperature. Finally, the cells were washed three times with PBS, mounted in Fluoromount G (Southern Biotechnology Associates, Birmingham, AL), and observed at 488−500 nm excitation and 510−550 nm emission wavelengths using a Nikon ECLIPSE E600 multiple microscope (Nikon, Melville, NY).

Transmembrane Predictions. The predicted topology structure models of BCRP were determined using the MEMSAT ((*44*)) (http://saier-144-37.ucsd.edu/memsat.html), PHDhtm (http://www.predictprotein.org), TopPred (http://mobyle.pasteur.fr/cgi-bin/MobylePortal/portal.py?form=toppred), HMMTOP ((*45*)) (http://www.enzim.hu/hmmtop), and SOSUI ((*46*)) (http://sosui.proteome.bio.tuat.ac.jp) algorithms.

Statistical Analysis. Efflux activities were presented as means ± SD of three independent experiments. Data were analyzed using one-way ANOVA analysis followed by the Student's *t*-test or only the Student's *t*-test to compare the activities of wild-type BCRP and the HA-tagged BCRP mutants. Differences with p values <0.05 were considered statistically significant.

RESULTS

Construction and Expression of HA-tagged BCRP Mutants. To determine membrane topology using the epitope insertion and indirect immunofluorescence approach, selection of insertion sites is critical. To map the intracellular and extracellular loops in a MSD as well as the location of the amino and carboxyl termini of the MSD, the insertion sites would be best selected in hydrophilic regions of the MSD. Therefore, we first performed hydropathy analysis of BCRP to identify putative hydrophilic regions in the MSD of BCRP. Hydropathy analysis according to Kyte and Doolittle (*47*) suggested that BCRP consists of a NBD (residues ∼1−395) followed by a MSD (residues ∼396−655), and the MSD likely contains 6 TM segments (Figure 1). This analysis generated a topology model very similar to that predicted using various algorithms as shown in Figure 5A (data not shown). Based on this analysis, we inserted HA epitope tags, one at a time, at 14 discrete positions in the predicted hydrophilic regions between TM segments and at the two ends of the MSD using PCR mutagenesis. Thus, HA epitope tags were inserted immediately after the amino acid residues 387 (construct 1), 420 (construct 2), 423 (construct 3), 454 (construct 4), 462 (construct 5), 474 (construct 6), 499 (construct 7), 502 (construct 8), 529 (construct 9), 532 (construct 10), 560 (construct 11), 594 (construct 12), 623 (construct 13), and 651 (construct 14) (Table 1). Approximate locations of these HA tags in BCRP are shown in Figure 1.

The pcDNA3.1 constructs containing wild-type BCRP and HA-tagged BCRP mutant cDNAs were then transiently transfected into HEK cells. Expression of BCRP proteins was analyzed by immunoblotting of whole cell lysates prepared from transfected cells (Figure 2). Immunoblotting using the BCRP-specific mAb BXP-21 could detect wild-type BCRP and several but not all of the BCRP mutants (Figure 2A). To further verify expression of HA-tagged BCRP mutants, we performed immunoblotting using an anti-BCRP polyclonal antibody. Specific bands of approximately 75 kDa were detected for wild-type BCRP and all of the mutants at comparable levels using the polyclonal antibody (Figure 2B). We then analyzed the same protein samples using a mAb specifically against the HA tag (Figure 2C). As expected, immunoreactive bands of approximately 75 kDa were observed in the samples prepared from cells transfected with all of the constructs carrying HA-tagged BCRP mutant cDNAs but were absent in the samples isolated from cells transfected with either the pcDNA3.1 empty vector or wild-type human *BCRP* cDNA (Figure 2C). These results suggest that all of the HA-tagged BCRP mutants were expressed in HEK cells at levels comparable to wild-type BCRP; however, some of the mutants could not be detected using the mAb BXP-21.

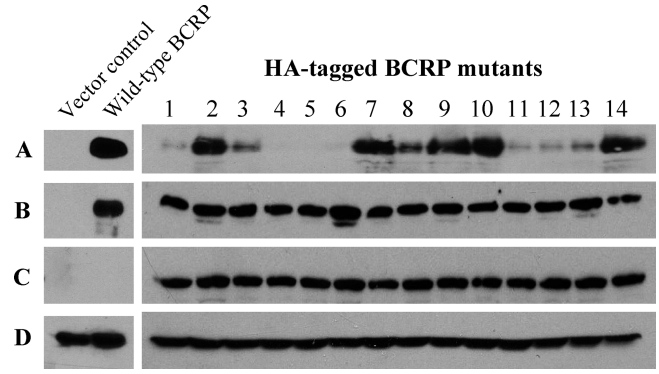

FIGURE 2: Immunoblots of HEK cells transfected with wild-type BCRP and HA-tagged BCRP mutant cDNA constructs 1−14. Whole cell lysates (30 μg of protein each lane) prepared from HEK cells transfected with wild-type BCRP and HA-tagged BCRP mutant cDNAs were immunoblotted, and BCRP was detected with mAb BXP-21 (A), a BCRP-specific polyclonal antibody (B), and a HA-specific mAb 12CA5 (C). β-Actin expression was also examined as internal control (D). The constructs are indicated by the numbers above the blots. Vector control and wild-type BCRP mean the blots of the samples prepared from cells transfected with the pcDNA3.1 empty vector and the expression vector containing full-length wild-type human *BCRP* cDNA, respectively. The experiments were repeated twice, and similar results were obtained.

Efflux Activities of HA-Tagged BCRP Mutants. We next examined the effects of HA tag insertion on BCRP efflux activity. Flow cytometric efflux assays were carried out with two known BCRP substrates, MX and BODIPY-prazosin (*43, 48*). The differences in intracellular MX or BODIPY-prazosin fluorescence between the cells in the presence and absence of the BCRP-specific inhibitor FTC were used to express FTC-inhibitable efflux activities of the cells expressing wild-type BCRP or HA-tagged BCRP mutants. As shown in Figure 3A, the MX efflux activities of the cells expressing wild-type BCRP were significantly increased approximately 6-fold compared with the activities associated with the vector control cells, indicating that BCRP effectively effluxes MX. The mutants with HA tag insertions at residues 454 (construct 4), 529 (construct 9), and 532 (construct 10) exhibited MX efflux activities comparable to wild-type BCRP. The mutants

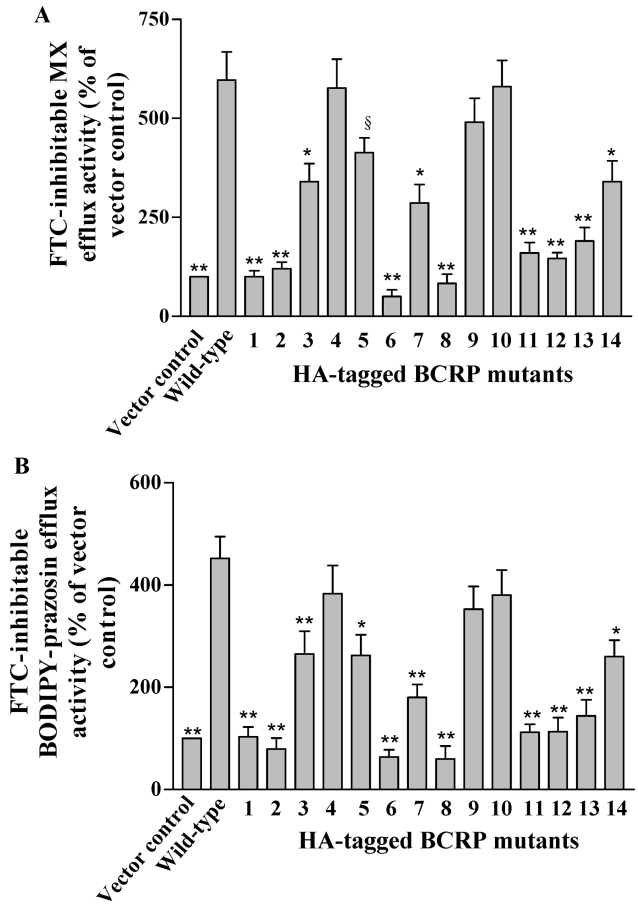

FIGURE 3: Efflux of MX and BODIPY-prazosin by wild-type BCRP and HA-tagged BCRP mutants. FTC-inhibitable MX (A) and BODIPY-prazosin (B) efflux activities of the cells transfected with wild-type BCRP and HA-tagged BCRP mutant cDNAs were measured using the flow cytometric efflux assay as described in Experimental Procedures. All of the activities were normalized to the activities associated with the vector control cells which were set as 100%. The results shown are means ± SD of three independent experiments. Significant difference: *, $p < 0.05$, and **, $p < 0.01$, as compared with wild-type BCRP by one-way ANOVA analysis followed by the Student's *t*-test; §, $p < 0.05$ as compared with wild-type BCRP by the Student's *t*-test. The constructs for HA-tagged BCRP mutants are indicated by numbers 1−14. Vector control and wild-type mean efflux activities of the cells transfected with the pcDNA3.1 empty vector and the expression vector containing full-length wild-type human *BCRP* cDNA, respectively.

with insertions at residues 423 (construct 3), 462 (construct 5), 499 (construct 7), and 651 (construct 14) retained approximately 50% of the wild-type BCRP activity. However, the MX efflux activities of the mutants with insertions at residues 560 (construct 11), 594 (construct 12), and 623 (construct 13) were reduced to approximately 10−20% of the wild-type BCRP activity, and the mutants with insertions at residues 387 (construct 1), 420 (construct 2), 474 (construct 6), and 502 (construct 8) were nearly completely inactive in transporting MX (Figure 3A). Similar results were obtained for BODIPY-prazosin (Figure 3B). These data suggest that, except for constructs 1, 2, 6, and 8, transfection of all other constructs produced functionally active BCRP mutants, although the BCRP-mediated efflux activities associated with the cells transfected with constructs 11, 12, and 13 were reduced to only 10−20% of the wild-type BCRP activity.

Localization of HA Epitope Tags. We then determined the membrane polarity (intracellular or extracellular) of the inserted HA tags by immunofluorescence analysis of HEK cells expressing HA-tagged BCRP mutants using an HA tag-specific mAb 12CA5. Immunofluorescence analysis was performed with intact cells or cells that had been permeabilized with Triton X-100 to determine extracellular or intracellular location of the tags, respectively. First of all, no cell-based fluorescence was detected in intact or permeabilized nontranfected control cells (data not shown) or in cells expressing wild-type BCRP (Figure 4A,F). A strong immunofluorescence signal was detected in both intact and permeabilized cells expressing the mutants with HA tag insertions at residues 420 (construct 2, Figure 4C,H), 423 (construct 3, Figure 4D,I), 454 (construct 4, Figure 4E,J), 499 (construct 7, Figure 4M,R), 502 (construct 8, Figure 4N,S), 594 (construct 12, Figure 4W,&), and 623 (construct 13, Figure 4X,Σ), suggesting the extracellular location of the HA tags in these BCRP mutants. The data also indicate that these HA tags are located in regions of the BCRP protein that are readily accessible to the antibody. In contrast, cells expressing the mutants with HA tag insertions at residues 387 (construct 1, Figure 4B), 474 (construct 6, Figure 4L), 529 (construct 9, Figure 4O), 532 (construct 10, Figure 4U), 560 (construct 11, Figure 4V), and 651 (construct 14, Figure 4Y) showed bright fluorescence only in permeabilized cells but not in intact, nonpermeabilized cells. This demonstrates the intracellular location of the HA tags in these BCRP mutants. The fluorescence signal associated with the mutant with the HA tag insertion at residue 462 (construct 5) was rather weak and could be barely detected only in permeabilized cells (Figure 4K), suggesting that this HA tag is likely situated in a region with limited accessibility to the antibody. For all of the mutants, fluorescence staining was mainly observed in the plasma membrane (Figure 4). This suggests that these mutants were predominantly targeted to the plasma membrane of HEK cells, although the possibility that a minor fraction is also present in intracellular membranes cannot be excluded. To confirm their plasma membrane expression, we performed confocal microscope analysis for several of the mutants, and the conclusion remained essentially the same (data not shown).

DISCUSSION

TM predictions using various algorithms suggest that BCRP consists of a NBD followed by a MSD which contains 6 or 7 TM segments, and the arrangement of TM segments varies substantially, depending on the algorithm used (Figure 5A−C). To confirm the predicted features of these models, we opted to determine the membrane topology of BCRP by HA tag insertion and indirect immunofluorescence. Results obtained from this study indicate that HA tags inserted at residues 420, 423, 454, 499, 502, 594, and 623 are located extracellularly, and HA tags inserted at residues 387, 474, 529, 532, 560, and 651 are situated in the intracellular regions of the MSD (Figure 4). On the basis of these experimental data combined with computer-prediction results, we deduced a membrane topology model for BCRP as shown in Figure 5D.

Epitope insertion may affect topogenesis of TM segments near the insertion sites by altering protein maturation, folding, expression, and/or targeting to the plasma membrane, which

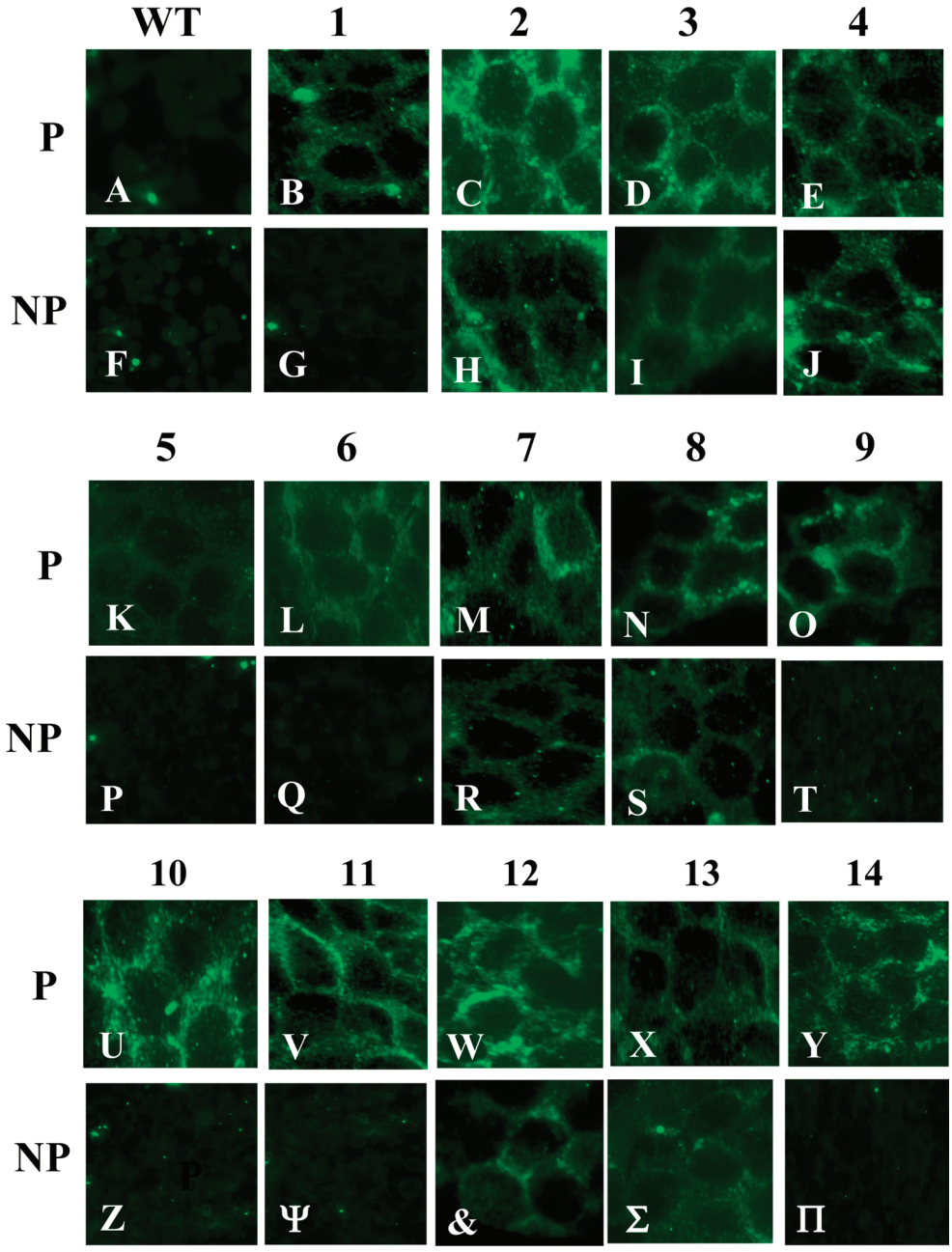

FIGURE 4: Immunofluorescence micrographs of HEK cells transfected with wild-type BCRP and HA-tagged BCRP mutant cDNA constructs. Cells were transfected with wild-type BCRP and HA-tagged BCRP mutant cDNAs, probed with the HA-specific mAb 12CA5, and processed for fluorescence microscopy as described in Experimental Procedures. The HA-tagged BCRP signals are indicated in green. Exposure times were identical for all of the micrographs. The HA tags in constructs 2 (C, H), 3 (D, I), 4 (E, J), 7 (M, R), 8 (N, S), 12 (W, &), and 13 (X, Σ) were detected in both permeabilized (P) and intact, nonpermeabilized (NP) cells, whereas the HA tags in constructs in 1 (B, G), 5 (K, P), 6 (L, Q), 9 (O, T), 10 (U, Z), 11 (V, Ψ), and 14 (Y, Π) were detected only in permeabilized cells. The corresponding constructs are shown in numbers 1−14 above the micrographs. Wild-type BCRP (A, F) was analyzed as a control. The experiments were repeated twice, and similar results were obtained.

could make the assignment of particularly intracellular epitopes uncertain. The immunofluorescence data clearly suggest that all of the HA-tagged BCRP mutants were predominately targeted to the plasma membrane of HEK cells (Figure 4). The immunoblotting results also indicate that the protein stability and expression of all the mutants were not affected by tag insertion (Figure 2B,C). These results suggest that the protein stability, maturation, expression, and targeting to the plasma membrane remained largely unaffected by tag insertion for all of these mutants. The mutants with HA tags at residues 423, 454, 462, 499, 529, 532, 560, 594, 623, and 651 were fully or at least partially active in transporting BCRP substrates (Figure 3), further confirming that sufficient amounts of these mutants were correctly folded and targeted to the plasma membrane to convey efflux activity.

Although the mutant with the HA tag at residue 387 was functionally inactive (Figure 3), the intracellular location of the tag determined in this study is consistent with the data from previous studies (*10, 49*). The immunofluorescence analysis in these studies using monoclonal or polyclonal antibodies raised against peptides in the predicted NBD (e.g., the peptide sequence 271−396 for BXP-21 (*10*); the peptide sequence 56−70 for the antibody 405 (*49*)) clearly revealed an intracellular location of the NBD. Since residue 387 is in

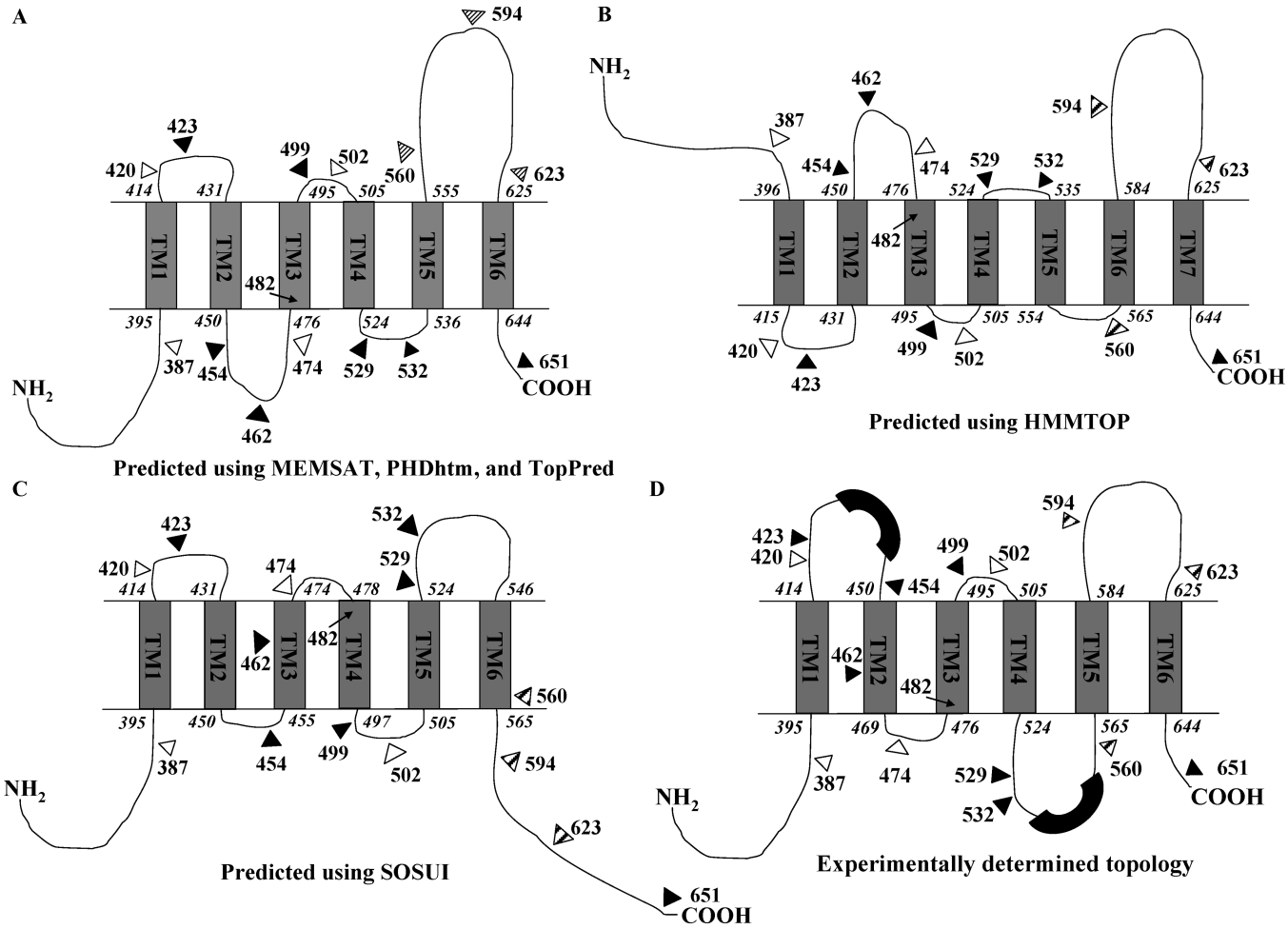

FIGURE 5: Topology models of BCRP. Solid, hatched, and open triangles indicate approximate positions of HA tag insertions that resulted in functional (with 50% or more of wild-type BCRP activity), partially functional (with less than 50% of wild-type BCRP activity), and inactive BCRP mutant proteins, respectively. (A) A model with 6 TM segments predicted using the MEMSAT, PHDhtm, and TopPred algorithms. (B) A model with 7 TM segments predicted using the HMMTOP algorithm. (C) A model with 6 TM segments predicted using the SOSUI algorithm. Note that the SOSUI algorithm does not predict the orientation of the termini of membrane proteins. Here we assign both the amino and carboxyl termini of BCRP an intracellular orientation in the SOSUI model as the NBD is unlikely located outside of the plasma membrane. (D) A model deduced from the results of mapping the inserted HA tags reported in this study. The approximate locations of residue 482 in the models are indicated by arrows. The coordinate positions of the residue numbers that delimit the approximate start and end of each TM are indicated in italic in these models. Approximate locations of the computer-predicted TM2 and TM5 from (A) in the intracellular or extracellular loop of the experimentally determined model are indicated with dark bell-shaped boxes.

close proximity to the NBD, it is unlikely that this residue is located outside of the plasma membrane. As to why the mutant is inactive is unclear. We hypothesize that residue 387 is possibly located in or close to a linker region connecting the NBD and the MSD which may be essential for the communication between the two domains (*50*). Insertion of the HA tag at this particular location could interrupt the communication between the NBD and the MSD and hence the overall transport activity of BCRP. In the homology model of Hazai and Bikadi (*34*), residue 387 is indeed located between the NBD and the MSD at a position close to the cytosolic surface of TM1. We also localized residue 651 in an intracellular region (Figure 4Y). Taken together, our data indicate that both the amino and carboxyl termini of the MSD of BCRP are located intracellularly.

In contrast, we localized the amino acid sequence 594−623 to the extracellular side of the plasma membrane (Figure 5D). This is in agreement with previous studies that identified only one residue (asparagine 596) as the glycosylation site (*51*). HA tag insertions at residues 594 and 623 did not seem to affect glycosylation as the bands of these mutants migrated to the similar positions as wild-type BCRP and other mutants (Figure 2). However, HA tag insertions at residues 594 and 623 significantly reduced the efflux activity, suggesting that the extracellular loop connecting TM5 and TM6 may play an important role in BCRP function. The recent studies indeed suggested that this extracellular loop may be critical in modulating substrate binding (*52*) as well as stability and ubiquitin-mediated degradation of BCRP (*53*).

HA tag insertions at residues 420, 474, and 502 completely abrogated the efflux activity (Figure 3) despite their proper targeting to the plasma membrane (Figure 4). We speculate that these residues are likely in close proximity to TM segments, and therefore HA tag insertions at these positions may affect the configuration of the nearby TM segments. Alternatively, these residues may just be critical for BCRP function (e.g., substrate binding and translocation). The observation of such inactive mutants does not exclude the conclusion that the amino acid sequence 420−454 is part of an extracellular loop connecting TM1 and TM2 (Figure 5D), as the mutants with HA tags at residues 423 and 454 were fully active (Figure 3) and readily observed in both perme-

abilized and intact cells by immunofluorescence (Figure 4). Likewise, the sequence 499−502 was localized to an extracellular loop connecting TM3 and TM4 (Figure 5D), as the mutant with the HA tag at residue 499 was functionally active (Figure 3) and readily observed in both permeabilized and intact cells by immunofluorescence (Figure 4). Since a TM segment usually contains approximately 20 amino acid residues, and the immunofluorescence data suggest an intracellular location for residue 474 (Figure 4L), we conclude that residue 474 is located in the intracellular loop connecting TM2 and TM3 (Figure 5D). As for residue 462, we noted that it was barely detectable only in permeabilized cells (Figure 4K), suggesting that this residue is likely buried in TM2 with limited accessibility to the antibody. Alternatively, TM2 may be a rather short TM segment, and hence residue 462 is located in a close proximity to the carboxyl terminus of TM2. Surprisingly, HA tag insertion at residue 462 did not drastically affect efflux activity of BCRP (Figure 3), even though such an insertion would be expected to distort the configuration of TM2. The reason for this observation remains to be determined. According to the experimentally determined model, residue 482 which is an important determinant of substrate specificity (*27, 29, 30, 33*) is located within TM3 at a position close to the cytosolic surface of the plasma membrane (Figure 5D). This is fully consistent with previous predictions (*29, 30, 33*). In the model of Hazai and Bikadi (*34*), residue 482 is similarly located close to the amino terminus of TM3 and points toward the interior of a substrate-binding cavity. Thus, our topology model is also consistent with the homology model with respect to the location of residue 482.

Results of the present study help to discriminate between several of the computer-generated topology models. The present study suggests that both the amino and carboxyl termini of the MSD of BCRP are located intracellularly (Figure 5D). In general, if the amino and carboxyl termini of a polytopic membrane protein are located at the same side of the membrane, it implies that there is an even number of TM segments in the protein. This essentially eliminates the HMMTOP model which predicts a 7-TM model for BCRP (Figure 5B). Although the SOSUI model contains 6 TM segments (Figure 5C), the locations of various residues in the model are not consistent with the results of this study. For example, residues 529 and 532 were localized in this study in the intracellular loop connecting TM4 and TM5; however, these residues in the SOSUI model were predicted to be in the extracellular loop connecting TM5 and TM6. The SOSUI algorithm also predicts that the amino acid sequence 594−623 is intracellular, which is impossible as the asparagine residue 596 is a glycosylation site (*51*). The MEMSAT, PHDhtm, and TopPred algorithms predict a topology model (Figure 5A) similar to the experimentally determined model (Figure 5D) but differing significantly in the arrangement of TM2 and TM5. Residues 454 and 462 were predicted in the intracellular loop connecting TM2 and TM3 but were experimentally localized in the extracellular loop connecting TM1 and TM2 and within TM2, respectively. Residue 560 was predicted in the extracellular loop connecting TM5 and TM6 but was determined to be situated in the intracellular loop connecting TM4 and TM5. Residues 529 and 532 were also localized intracellularly (Figure 4). These results depict a relatively large intracellular loop connecting TM4 and TM5. Hydropathy analysis indicates that a large portion of this loop is as hydrophobic as a TM segment (Figure 1), which suggests possible hydrophobic helical packing of the loop. It is worthwhile to mention that, in the model of Hazai and Bikadi (*34*), the loop connecting TM4 and TM5 is much shorter and forms α-helices extending from the TM segments. A similar situation applies to the extracellular loop connecting TM1 and TM2.

Despite the significant similarity shared between the experimentally determined model (Figure 5D) and those obtained using computer-prediction (Figure 5A) and homologue modeling (*34*) in the number of TM segments, the orientation of the amino and carboxyl termini of the MSD, and the length and positioning of TM1, TM3, TM4, and TM6, a major difference among these models is the shift of TM2 and TM5. Although it needs to be further clarified in future studies, such an arrangement of TM2 and TM5 as illustrated in Figure 5D seems possible. First, Hazai and Bikadi (*34*) predicted that TM5 is formed from residues 545−564. However, one-third of TM5 (residues 553−559) were not predicted to form an α-helix (*34*), which seems unlikely for a TM α-helical segment. Second, the amino acid residues of TM2 and TM5 of the experimentally determined model (450−469 and 565−584, respectively) were predicted to form α-helices, with the exception of only three residues 462−464 (*34*). Furthermore, although the overall topology structures predicted using the HMMTOP and SOSUI algorithms seem unlikely, residues 565−584 were predicted to form a TM segment (Figure 5B) and a large part of residues 450−469 was predicted to be in a TM segment (Figure 5C), suggesting the likelihood of these residues themselves to form TM α-helices by nature. Consistent with this, the prediction of TM2 and TM5 in the homology modeling studies (*34, 35*) was clearly much more uncertain than other TM segments. Finally, in spite of the relatively high hydrophilicity of some residues in regions 450−469 and 565−584, they could penetrate the lipid bilayer if they are shielded away from exposure to hydrophobic acyl chains of lipids or point toward the interior of the substrate-binding cavity. Similar observations have been made with P-glycoprotein in which some of the predicted TM segments were determined to be located in the intracellular or extracellular loops (*54, 55*).

In summary, we have provided the first direct experimental evidence in support of a 6-TM model for BCRP which is consistent with the currently available biochemical data. This new topology model may have important implications for further understanding of the interactions of drugs with BCRP and the transport mechanism of this medically important drug transporter.

ACKNOWLEDGMENT

We thank Dr. Susan E. Bates (National Cancer Institute, Bethesda, MD) for providing the full-length wild-type human *BCRP* cDNA. We also acknowledge Mr. Greg Martin (The Keck Imaging Center, University of Washington) for technical help in immunofluorescence microscopy.

REFERENCES

1. Miyake, K., Mickley, L., Litman, T., Zhan, Z., Robey, R., Cristensen, B., Brangi, M., Greenberger, L., Dean, M., Fojo, T., and Bates, S. E. (1999) Molecular cloning of cDNAs which are

highly overexpressed in mitoxantrone-resistant cells: demonstration of homology to ABC transport genes. *Cancer Res. 59*, 8–13.
2. Doyle, L. A., and Ross, D. D. (2003) Multidrug resistance mediated by the breast cancer resistance protein BCRP (ABCG2). *Oncogene 22*, 7340–7358.
3. Robey, R. W., Polgar, O., Deeken, J., To, K. W., and Bates, S. E. (2007) ABCG2: determining its relevance in clinical drug resistance. *Cancer Metastasis Rev. 26*, 39–57.
4. Doyle, L. A., Yang, W., Abruzzo, L. V., Krogmann, T., Gao, Y., Rishi, A. K., and Ross, D. D. (1998) A multidrug resistance transporter from human MCF-7 breast cancer cells. *Proc. Natl. Acad. Sci. U.S.A. 95*, 15665–15670.
5. Allikmets, R., Schriml, L. M., Hutchinson, A., Romano-Spica, V., and Dean, M. (1998) A human placenta-specific ATP-binding cassette gene (ABCP) on chromosome 4q22 that is involved in multidrug resistance. *Cancer Res. 58*, 5337–5339.
6. Mao, Q., and Unadkat, J. D. (2005) Role of the breast cancer resistance protein (ABCG2) in drug transport. *Aaps J. 7*, E118−E133.
7. Polgar, O., Robey, R. W., and Bates, S. E. (2008) ABCG2: structure, function and role in drug response. *Expert Opin. Drug Metab. Toxicol. 4*, 1–15.
8. Krishnamurthy, P., and Schuetz, J. D. (2006) Role of ABCG2/BCRP in biology and medicine. *Annu. Rev. Pharmacol. Toxicol. 46*, 381–410.
9. Calcagno, A. M., Kim, I. W., Wu, C. P., Shukla, S., and Ambudkar, S. V. (2007) ABC drug transporters as molecular targets for the prevention of multidrug resistance and drug-drug interactions. *Curr. Drug Deliv. 4*, 324–333.
10. Maliepaard, M., Scheffer, G. L., Faneyte, I. F., van Gastelen, M. A., Pijnenborg, A. C., Schinkel, A. H., van De Vijver, M. J., Scheper, R. J., and Schellens, J. H. (2001) Subcellular localization and distribution of the breast cancer resistance protein transporter in normal human tissues. *Cancer Res. 61*, 3458–3464.
11. Zhou, L., Naraharisetti, S. B., Wang, H., Unadkat, J. D., Hebert, M. F., and Mao, Q. (2008) The breast cancer resistance protein (Bcrp1/Abcg2) limits fetal distribution of glyburide in the pregnant mouse: an Obstetric-Fetal Pharmacology Research Unit Network and University of Washington Specialized Center of Research Study. *Mol. Pharmacol. 73*, 949–959.
12. Kruijtzer, C. M., Beijnen, J. H., Rosing, H., ten Bokkel Huinink, W. W., Schot, M., Jewell, R. C., Paul, E. M., and Schellens, J. H. (2002) Increased oral bioavailability of topotecan in combination with the breast cancer resistance protein and P-glycoprotein inhibitor GF120918. *J. Clin. Oncol. 20*, 2943–2950.
13. Merino, G., Jonker, J. W., Wagenaar, E., van Herwaarden, A. E., and Schinkel, A. H. (2005) The breast cancer resistance protein (BCRP/ABCG2) affects pharmacokinetics, hepatobiliary excretion, and milk secretion of the antibiotic nitrofurantoin. *Mol. Pharmacol. 67*, 1758–1764.
14. Jonker, J. W., Smit, J. W., Brinkhuis, R. F., Maliepaard, M., Beijnen, J. H., Schellens, J. H., and Schinkel, A. H. (2000) Role of breast cancer resistance protein in the bioavailability and fetal penetration of topotecan. *J. Natl. Cancer Inst. 92*, 1651–1656.
15. Zhang, W., Yu, B. N., He, Y. J., Fan, L., Li, Q., Liu, Z. Q., Wang, A., Liu, Y. L., Tan, Z. R., Fen, J., Huang, Y. F., and Zhou, H. H. (2006) Role of BCRP 421C→A polymorphism on rosuvastatin pharmacokinetics in healthy Chinese males. *Clin. Chim. Acta 373*, 99–103.
16. Yamasaki, Y., Ieiri, I., Kusuhara, H., Sasaki, T., Kimura, M., Tabuchi, H., Ando, Y., Irie, S., Ware, J., Nakai, Y., Higuchi, S., and Sugiyama, Y. (2008) Pharmacogenetic characterization of sulfasalazine disposition based on NAT2 and ABCG2 (BCRP) gene polymorphisms in humans. *Clin. Pharmacol. Ther. 84*, 95–103.
17. Urquhart, B. L., Ware, J. A., Tirona, R. G., Ho, R. H., Leake, B. F., Schwarz, U. I., Zaher, H., Palandra, J., Gregor, J. C., Dresser, G. K., and Kim, R. B. (2008) Breast cancer resistance protein (ABCG2) and drug disposition: intestinal expression, polymorphisms and sulfasalazine as an in vivo probe. *Pharmacogenet. Genomics 18*, 439–448.
18. Zhang, Y., Wang, H., Unadkat, J. D., and Mao, Q. (2007) Breast cancer resistance protein 1 limits fetal distribution of nitrofurantoin in the pregnant mouse. *Drug Metab. Dispos. 35*, 2154–2158.
19. Jonker, J. W., Merino, G., Musters, S., van Herwaarden, A. E., Bolscher, E., Wagenaar, E., Mesman, E., Dale, T. C., and Schinkel, A. H. (2005) The breast cancer resistance protein BCRP (ABCG2) concentrates drugs and carcinogenic xenotoxins into milk. *Nat. Med. 11*, 127–129.
20. van Herwaarden, A. E., Wagenaar, E., Merino, G., Jonker, J. W., Rosing, H., Beijnen, J. H., and Schinkel, A. H. (2007) Multidrug transporter ABCG2/breast cancer resistance protein secretes riboflavin (vitamin B2) into milk. *Mol. Cell. Biol. 27*, 1247–1253.
21. Xu, J., Liu, Y., Yang, Y., Bates, S., and Zhang, J. T. (2004) Characterization of oligomeric human half-ABC transporter ATP-binding cassette G2. *J. Biol. Chem. 279*, 19781–19789.
22. McDevitt, C. A., Collins, R. F., Conway, M., Modok, S., Storm, J., Kerr, I. D., Ford, R. C., and Callaghan, R. (2006) Purification and 3D structural analysis of oligomeric human multidrug transporter ABCG2. *Structure 14*, 1623–1632.
23. Bhatia, A., Schafer, H. J., and Hrycyna, C. A. (2005) Oligomerization of the human ABC transporter ABCG2: evaluation of the native protein and chimeric dimers. *Biochemistry 44*, 10893–10904.
24. Robey, R. W., Honjo, Y., Morisaki, K., Nadjem, T. A., Runge, S., Risbood, M., Poruchynsky, M. S., and Bates, S. E. (2003) Mutations at amino-acid 482 in the ABCG2 gene affect substrate and antagonist specificity. *Br. J. Cancer 89*, 1971–1978.
25. Polgar, O., Ozvegy-Laczka, C., Robey, R. W., Morisaki, K., Okada, M., Tamaki, A., Koblos, G., Elkind, N. B., Ward, Y., Dean, M., Sarkadi, B., and Bates, S. E. (2006) Mutational studies of G553 in TM5 of ABCG2: a residue potentially involved in dimerization. *Biochemistry 45*, 5251–5260.
26. Polgar, O., Robey, R. W., Morisaki, K., Dean, M., Michejda, C., Sauna, Z. E., Ambudkar, S. V., Tarasova, N., and Bates, S. E. (2004) Mutational analysis of ABCG2: role of the GXXXG motif. *Biochemistry 43*, 9448–9456.
27. Miwa, M., Tsukahara, S., Ishikawa, E., Asada, S., Imai, Y., and Sugimoto, Y. (2003) Single amino acid substitutions in the transmembrane domains of breast cancer resistance protein (BCRP) alter cross resistance patterns in transfectants. *Int. J. Cancer 107*, 757–763.
28. Tamura, A., Wakabayashi, K., Onishi, Y., Takeda, M., Ikegami, Y., Sawada, S., Tsuji, M., Matsuda, Y., and Ishikawa, T. (2007) Re-evaluation and functional classification of non-synonymous single nucleotide polymorphisms of the human ATP-binding cassette transporter ABCG2. *Cancer Sci. 98*, 231–239.
29. Ozvegy-Laczka, C., Koblos, G., Sarkadi, B., and Varadi, A. (2005) Single amino acid (482) variants of the ABCG2 multidrug transporter: major differences in transport capacity and substrate recognition. *Biochim. Biophys. Acta 1668*, 53–63.
30. Honjo, Y., Hrycyna, C. A., Yan, Q. W., Medina-Perez, W. Y., Robey, R. W., van de Laar, A., Litman, T., Dean, M., and Bates, S. E. (2001) Acquired mutations in the MXR/BCRP/ABCP gene alter substrate specificity in MXR/BCRP/ABCP-overexpressing cells. *Cancer Res. 61*, 6635–6639.
31. Henriksen, U., Gether, U., and Litman, T. (2005) Effect of Walker A mutation (K86M) on oligomerization and surface targeting of the multidrug resistance transporter ABCG2. *J. Cell Sci. 118*, 1417–1426.
32. Imai, Y., Nakane, M., Kage, K., Tsukahara, S., Ishikawa, E., Tsuruo, T., Miki, Y., and Sugimoto, Y. (2002) C421A polymorphism in the human breast cancer resistance protein gene is associated with low expression of Q141K protein and low-level drug resistance. *Mol. Cancer Ther. 1*, 611–616.
33. Allen, J. D., Jackson, S. C., and Schinkel, A. H. (2002) A mutation hot spot in the Bcrp1 (Abcg2) multidrug transporter in mouse cell lines selected for Doxorubicin resistance. *Cancer Res. 62*, 2294–2299.
34. Hazai, E., and Bikadi, Z. (2008) Homology modeling of breast cancer resistance protein (ABCG2). *J. Struct. Biol. 162*, 63–74.
35. Li, Y. F., Polgar, O., Okada, M., Esser, L., Bates, S. E., and Xia, D. (2007) Towards understanding the mechanism of action of the multidrug resistance-linked half-ABC transporter ABCG2: a molecular modeling study. *J. Mol. Graphics Model. 25*, 837–851.
36. Kast, C., Canfield, V., Levenson, R., and Gros, P. (1995) Membrane topology of P-glycoprotein as determined by epitope insertion: transmembrane organization of the N-terminal domain of mdr3. *Biochemistry 34*, 4402–4411.
37. Kast, C., and Gros, P. (1997) Topology mapping of the amino-terminal half of multidrug resistance-associated protein by epitope insertion and immunofluorescence. *J. Biol. Chem. 272*, 26479–26487.
38. Banerjee, A., and Swaan, P. W. (2006) Membrane topology of human ASBT (SLC10A2) determined by dual label epitope insertion scanning mutagenesis. New evidence for seven transmembrane domains. *Biochemistry 45*, 943–953.

39. Sone, M., and Orlow, S. J. (2007) The ocular albinism type 1 gene product, OA1, spans intracellular membranes 7 times. *Exp. Eye Res. 85*, 806–816.
40. Gama, L., and Breitwieser, G. E. (2002) Generation of epitope-tagged proteins by inverse polymerase chain reaction mutagenesis. *Methods Mol. Biol. 182*, 77–83.
41. Gupta, A., Zhang, Y., Unadkat, J. D., and Mao, Q. (2004) HIV protease inhibitors are inhibitors but not substrates of the human breast cancer resistance protein (BCRP/ABCG2). *J. Pharmacol. Exp. Ther. 310*, 334–341.
42. Wang, H., Lee, E. W., Zhou, L., Leung, P. C., Ross, D. D., Unadkat, J. D., and Mao, Q. (2008) Progesterone receptor (PR) isoforms PRA and PRB differentially regulate expression of the breast cancer resistance protein in human placental choriocarcinoma BeWo cells. *Mol. Pharmacol. 73*, 845–854.
43. Vethanayagam, R. R., Wang, H., Gupta, A., Zhang, Y., Lewis, F., Unadkat, J. D., and Mao, Q. (2005) Functional analysis of the human variants of breast cancer resistance protein: I206L, N590Y, and D620N. *Drug Metab. Dispos. 33*, 697–705.
44. Jones, D. T., Taylor, W. R., and Thornton, J. M. (1994) A model recognition approach to the prediction of all-helical membrane protein structure and topology. *Biochemistry 33*, 3038–3049.
45. Tusnady, G. E., and Simon, I. (1998) Principles governing amino acid composition of integral membrane proteins: application to topology prediction. *J. Mol. Biol. 283*, 489–506.
46. Hirokawa, T., Boon-Chieng, S., and Mitaku, S. (1998) SOSUI: classification and secondary structure prediction system for membrane proteins. *Bioinformatics 14*, 378–379.
47. Kyte, J., and Doolittle, R. F. (1982) A simple method for displaying the hydropathic character of a protein. *J. Mol. Biol. 157*, 105–132.
48. Robey, R. W., Honjo, Y., van de Laar, A., Miyake, K., Regis, J. T., Litman, T., and Bates, S. E. (2001) A functional assay for detection of the mitoxantrone resistance protein, MXR (ABCG2). *Biochim. Biophys. Acta 1512*, 171–182.
49. Litman, T., Jensen, U., Hansen, A., Covitz, K. M., Zhan, Z., Fetsch, P., Abati, A., Hansen, P. R., Horn, T., Skovsgaard, T., and Bates, S. E. (2002) Use of peptide antibodies to probe for the mitoxantrone resistance-associated protein MXR/BCRP/ABCP/ABCG2. *Biochim. Biophys. Acta 1565*, 6–16.
50. Sarkadi, B., Homolya, L., Szakacs, G., and Varadi, A. (2006) Human multidrug resistance ABCB and ABCG transporters: participation in a chemoimmunity defense system. *Physiol. Rev. 86*, 1179–1236.
51. Mohrmann, K., van Eijndhoven, M. A., Schinkel, A. H., and Schellens, J. H. (2005) Absence of N-linked glycosylation does not affect plasma membrane localization of breast cancer resistance protein (BCRP/ABCG2). *Cancer Chemother. Pharmacol. 56*, 344–350.
52. Ozvegy-Laczka, C., Laczko, R., Hegedus, C., Litman, T., Varady, G., Goda, K., Hegedus, T., Dokholyan, N. V., Sorrentino, B. P., Varadi, A., and Sarkadi, B. (2008) Interaction with the 5D3 monoclonal antibody is regulated by intramolecular rearrangements but not by covalent dimer formation of the human ABCG2 multidrug transporter. *J. Biol. Chem. 283*, 26059–26070.
53. Wakabayashi, K., Nakagawa, H., Tamura, A., Koshiba, S., Hoshijima, K., Komada, M., and Ishikawa, T. (2007) Intramolecular disulfide bond is a critical check point determining degradative fates of ATP-binding cassette (ABC) transporter ABCG2 protein. *J. Biol. Chem. 282*, 27841–27846.
54. Zhang, J. T., and Ling, V. (1991) Study of membrane orientation and glycosylated extracellular loops of mouse P-glycoprotein by in vitro translation. *J. Biol. Chem. 266*, 18224–18232.
55. Zhang, J. T., Duthie, M., and Ling, V. (1993) Membrane topology of the N-terminal half of the hamster P-glycoprotein molecule. *J. Biol. Chem. 268*, 15101–15110.

BI801644V